Unexpected structural properties in the saturation region of the odd-even effects in aliphatic polyethers: Influence of crystallization conditions

Irma Flores[1^], Ricardo A. Pérez-Camargo[2*], Elena Gabirondo[1], Maria Rosaria Caputo[1], Guoming Liu[2,3], Dujin Wang[2,3], Haritz Sardon[1], Alejandro J. Müller[1,4*]

[1]POLYMAT and Department of Polymers and Advanced Materials: Physics, Chemistry and Technology, Faculty of Chemistry, University of the Basque Country UPV/EHU, Paseo Manuel de Lardizabal 3, Donostia-San Sebastián 20018, Spain

[2]Beijing National Laboratory for Molecular Sciences, CAS Key Laboratory of Engineering Plastics, Institute of Chemistry, Chinese Academy of Sciences, Beijing 100190, China.

[3]University of Chinese Academy of Sciences, Beijing 100049, China

[4]IKERBASQUE, Basque Foundation for Science, Plaza Euskadi 5, Bilbao 48009, Spain.

*Corresponding authors: ricardo507@iccas.ac.cn, alejandrojesus.muller@ehu.es

^Dedicated to the memory of our beloved colleague and friend Dr. Irma Flores

For TOC

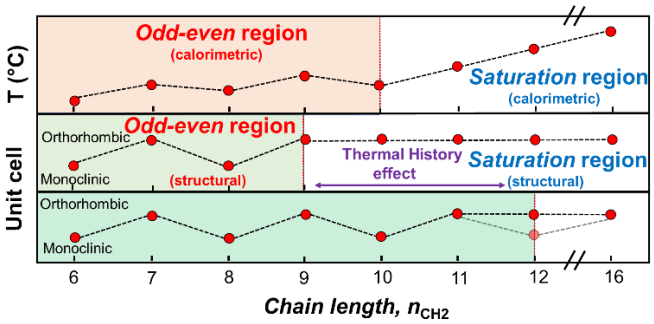
T (°C)
Odd-even region
(calorimetric)
Saturation region
(calorimetric)
Unit cell
Odd-even region
Orthorhombic
Monoclinic
(structural)
Thermal History
effect
Saturation region
(structural)
Orthorhombic
Monoclinic
6
7
8
9
10
11
12
16
Chain length, n_{CH2}

ABSTRACT

A series of aliphatic polyethers with different chain lengths (n_{CH2}= 6 to 12, and 16) is studied employing differential scanning calorimetry and X-rays scattering. The calorimetric and structural behavior of samples crystallized from the melt is divided into the *odd-even* and *saturation* regions. In the *odd-even* region (n_{CH2} = 6 to 10), the odd samples (n_{CH2} = 7, and 9) show enhanced calorimetric properties (e.g., higher transition temperatures) and faster crystallization kinetics than the even ones (n_{CH2} = 6, 8 and 10). The odd samples crystallize in orthorhombic unit cells and the even ones in monoclinic unit cells. In the *saturation* region (n_{CH2} = 11 to 16), the calorimetric properties increase as n_{CH2} increases without alternation. However, unexpectedly, the n_{CH2} = 12 displayed a mixed structure (monoclinic + orthorhombic) instead of an orthorhombic one. Thus, a structural saturation effect (i.e., an orthorhombic unit cell) is not reached. This particular structural feature was investigated under varied thermal histories, induced by different cooling rates. The samples as synthesized (i.e., crystallized during precipitation from solution) exhibited a structural saturation effect since both n_{CH2} = 10 and 12 display an orthorhombic unit cell. But, the n_{CH2} = 10 exhibits a monoclinic unit cell, and the n_{CH2} = 12 a mixed structure when the samples crystallize from the melt at different rates. Only the n_{CH2} = 16 crystallizes in an orthorhombic unit cell, independently of the thermal history. Thus, the complex odd-even effects in these aliphatic polyethers are a function of the cooling rate from the melt and sample preparation procedures (solution or melt crystallization).

Keywords: odd-even effect, saturation of the odd-even effect, rate-dependent behavior, structural alternation, odd-even effect limits.

1. Introduction

Polyethers have maintained continuous development despite a long history of research (around 170 years). Their main characteristic is the oxygen bridge between two organics (alkyl or aryl) residues.[1] In general, the aliphatic polyethers are defined as those containing ether groups in the saturated main chain.[2]

The ring-opening polymerization (ROP) of cyclic ethers (e.g., oxiranes, oxetanes, and tetrahydrurofuran[3-5]) is the most employed method to prepare aliphatic polyethers.[6, 7]. The ones with the most commercial interest are poly (ethylene glycol), poly (propylene glycol), and poly (tetrahydrofuran), PTHF. It is possible to find properties in these materials ranging from highly crystalline to amorphous ones, leading to a broad range of applications. The most important known applications are water-soluble surfactants, drug-delivery systems,[8] products for the automotive or electrical industry,[1] dry-solid polymer electrolytes,[9] soft-segments in polyurethane chemistry,[1, 10, 11] nanomedicine, among others.[6]

However, the ROP is limited to polyethers containing up to five units between ether linkages.[7] To obtain more units between ether linkages (i.e., more than 5 CH_2), alternative methods must be used due to the stability of medium-long chain cyclic ethers. Thus, Williamson etherification,[12] catalytic reduction of polyesters,[13] or the self-condensation of alcohols in the presence of a non-eutectic mixture organocatalyst (NEMO) [6, 7] have been explored for the production of medium-long chain polyethers. Among these methods, the latter one has recently allowed obtaining medium-long chain aliphatic polyethers, linear copolyethers, fully biobased copolyether polyols (polyurethanes chemistry),[11] glassy polyether,[14] and cross-linked aliphatic polyethers.[6, 7]

Recent works have synthesized aliphatic polyethers in a wide chain length range, n_{CH2} = 6 to 12. These materials showed semicrystalline behavior and melting point values from 54 to 85 °C depending on n_{CH2}, and two types of crystalline structures (i.e., PTHF- and polyethylene (PE)-type unit cell).[6] Additionally, the 1,6-hexanediol (C6) and 1,12-dodecanediol (C12) were copolymerized *via* a bulk self-condensation method (using a thermally stable NEMO) at high temperatures, obtaining C6-*ran*-C12 copolymers in a wide range of compositions. The C6-*ran*-C12 copolymers show an isomorphic behavior.[7] The isomorphism is a rare crystallization mode in random copolymers (see more details

in Reference 15). These studies show that the aliphatic polyethers have interesting properties and crystallization phenomena. One crystallization phenomenon that has not been intensely studied in aliphatic polyethers due to the n_{CH2} limitations is the even-odd effect.

The even-odd effect has been studied since the last century. Its main characteristic is the alternation (i.e., even vs. odd) of the solid-state physical properties (e.g., modulus and melting points) as n_{CH2} increases. In contrast, the liquid state properties (e.g., boiling points in low molecular weight materials) generally increase linearly as n_{CH2} increases. Although, recently, it has been pointed out that the viscosity near the melting point shows an alternating behavior as well. 16 The even-odd effect is very pronounced for specific materials, as (a) thermotropic liquid crystalline phases, (b) *n*-alkanes, and some *n*-alkyl derivatives at a relatively low number of CH_2 segments, and (c) in the presence of functional groups in both chain extremities compared to monosubstituted alkanes.17, 18 Also, this effect has been found in precision polymers.19 Most cases reported that the even members exhibit higher properties than the odd ones, but some works reported the opposite.20, 21 Here, we take the convention of referring to the former case (and most general one) as an even-odd effect and the opposite case as an odd-even effect.

Another characteristic of the even-odd effect is its disappearance, or saturation, due to the decreasing influence of the functional groups as the methylene sequence increases (i.e., increase of the n_{CH2}). The increasing influence of the methylene sequence makes the London dispersion interactions the critical factor (instead of the dipolar interactions of the functional groups) to the packing structure.19 Therefore, the materials in the saturation region resemble polyethylene (PE) in both structure and conformations. The saturation of the even-odd effect depends on the nature of the polymer (i.e., type of functional groups) and the n_{CH2} range studied. The saturation of the even-odd effect has been recently reported in aliphatic polycarbonates22 for $n_{CH2} > 9$, and precision polyacetals for $n_{CH2} > 10$.19 This effect has also been reported in arylate polyesters for $n_{CH2} = 15$, in which an all-*trans* conformation was obtained.23, 24 It is worth noting that for polyamides (PA)25 and polyurethanes,26 the even-odd effect is still present for n_{CH2} values as high as 12.

The even-odd effect has been related to a "packing effect". For instance, in *n*-alkanes, the packing effect is related to the intermolecular distance between the end-group, leading to a more efficient packing in the even samples than the odd ones,

producing, in the even members, higher densities and melting temperatures.[16] For end-substituted *n*-alkanes, where the substituent groups are diols and diamines, the packing effect is more evident due to hydrogen bonds and dispersive forces promoting it.[27] Another explanation for the even-odd effect is the conformation of the chains. In general, the even samples display an all-*trans* conformation that promotes a more efficient package.[18] For instance, in arylate polyesters, for n_{CH2} < 15, even samples exhibited an all-*trans* conformation, while odd ones displayed kinked conformations with the *gauche* bonds around the C(O)–O–CH_2CH_2 bonds[23, 24], explaining the even-odd effect. But, for those materials that cannot adopt an all-*trans* conformation, it is suggested that the ability of the CH_2 chains to adopt different conformations generates the even-odd effect.[18] The available conformations depend on kinetics barriers to exchange and intermolecular packing.[18]

For aliphatic polyamides (PA *X* and PA *XY*), the even-odd effect has been related to the capacity to form hydrogen bonds. For instance, PA*7* (i.e., six methylene groups in the repeating unit) can form all possible hydrogen bonds irrespective of the orientation of the neighboring chains (i.e., parallel and antiparallel orientations). In contrast, in PA*6* (i.e., five methylene groups in the repeating units), the hydrogen bonds can be formed when two neighboring chains adopt the antiparallel orientation. Thus, for PAs, the lack of complete hydrogen bonding for the odd members explained their lower melting points, despite a higher amide density, than the even members. In the case of the PA *XY* type, the even-even combination is more efficient packing than the odd-odd combination, explaining the higher melting points.[25] Despite the well-established general even-odd effect behavior, the study of new materials still bring highlights regarding the even-odd effect phenomena, which has been studied for one century.[28]

As far as the authors are aware, the odd-even effect in aliphatic polyethers has not been detected yet. However, structural characterization of these materials has been performed by Kobayashi et al.[29] They found different crystalline structures (i.e., PTHF vs. PE-type unit cell) for aliphatic polyethers with n_{CH2} = 4, 6 to 10, and 12, and detected that the melting temperatures (T_m) increase as n_{CH2} increases.[29] Similar results are reported by Basterretxea et al.[6] These authors reported that the first-order transitions (i.e., crystallization and melting temperatures) and the corresponding enthalpies increases as n_{CH2} increases. Structurally, those materials with n_{CH2} = 6 and 8 displayed a PTHF-type unit cell, whereas those with n_{CH2} = 7, 9 to 12 displayed a PE-type unit cell.[6] These works[6, 29] did not detect an even-odd effect and were not focused on it. Considering that,

in some cases, the even-odd effect is caused only by different packing patterns, without differences in the crystal structure,27 a complete characterization (i.e., that includes thermal and structural characterization) is needed to identify the even-odd effect of a particular system.

This work focuses on the thermal (through non-isothermal and isothermal experiments) and structural (through wide/small-angle X-ray scattering experiments) characterization of aliphatic polyethers. For this characterization, we have selected aliphatic polyethers with n_{CH2} = 6 to 12 and 16 to understand its odd-even effect.

2. Experimental Part

The synthesis of the materials was performed according to the procedure of Basterretxea et al.6 by a multistep polymerization process (*Step 1* at 130 ° C for 24 h, *Step 2* at 180 ° C for 24 h, and *Step 3* at 200 ° C for 24 h) using 5 mol% of a non-eutectic base organocatalyst [methanesulfonic acid (MSA): triazabicyclo [4.4.0]dec-5-ene (TBD)].6 Samples were purified by dissolving them in chloroform followed by precipitation in methanol. After drying, a powder sample was obtained (denoted "as synthesized" samples in this work). The different chain lengths or the number of methylene units in the main chain, n_{CH2}, were obtained by a diol self-condensing, changing the number of methylenes on it from 6 to 12, and 16. For more details, see the synthesis and chemical characterization in our previous work in reference 6. The obtained aliphatic polyethers are listed in Table 1 and schematically represented in Scheme 1.

Table 1. Aliphatic polyethers and their chemical characterization data.

Monomer	***Abbreviation***	***Chain length*** (n_{CH2})	M_n* **(g/mol)**	$Đ$*
1,6-hexanediol	C6	6	22000	1.9
1,7-heptanediol	C7	7	8000	2.3
1,8-octanediol	C8	8	18000	1.4
1,9-nonanediol	C9	9	9500	2.5
1,10-decanediol	C10	10	8500	2.5
1,11-undecanediol	C11	11	8000	2.3
1,12-dodecanediol	C12	12	5000	2.5
1,16-hexadecanediol	C16	16	1500+	–

* Average number molecular weight (M_n) and dispersity index ($Đ$)6 were determined by SEC in $CHCl_3$ except for 1,16-hexadecanediol+ (determined by NMR).

The chemical structure of the aliphatic polyethers studied in this work is shown in Scheme 1. These materials only differ in the chain length (n_{CH2}).

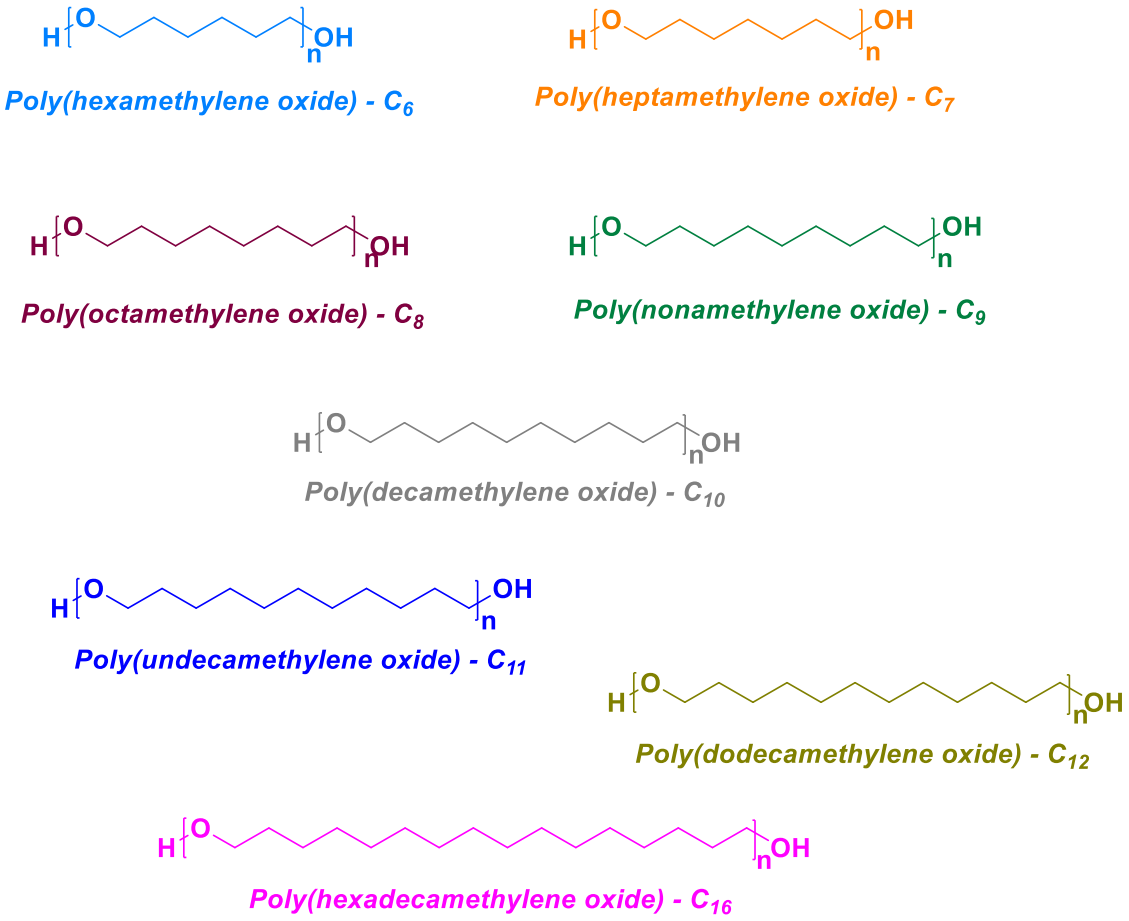

Scheme 1. Chemical structure of the different polyethers.

Differential Scanning Calorimetry (DSC)

The thermal behavior of the materials was determined with a DSC 8500 (PerkinElmer) connected to an Intracooler *III*. The experiments were performed under an ultrapure atmosphere generated with a nitrogen flow of 20 mL/min. The DSC 8500 was calibrated with tin and indium standards. The selected scanning rate was 20 °C/min, for both heating and cooling scans, in a temperature range of – 60 to 150 °C. Each sample weighed *circa* 5 mg.

Non-isothermal experiments were performed by heating the sample from RT to 150 °C, recording the first heating scan, and holding the sample, for 3 minutes, at this temperature to erase the thermal history. Subsequently, a cooling from 150 to – 60 °C was performed, recording the cooling scan. Finally, after 1 minute at – 60 °C, the sample was heated to 150 °C to register the second heating.

Isothermal experiments were performed following the recommended procedure by Lorenzo et al.30 Before the isothermal crystallization, the minimum isothermal crystallization temperature was determined ($T_{c,min}$), through a simple test. The samples were cooled from the melt to selected T_c, at a selected cooling rate (i.e., generally performed at 60 °C/min). Subsequently, a heating scan at 20 °C/min was performed. If an endotherm is detected during this heating, it implies that the sample can crystallize during the cooling step; hence, the selected T_c is not high enough to avoid the crystallization during the cooling step. Therefore, a $T_{c,min}$ can be defined in which the sample does not crystallize during the cooling step (i.e., no endotherm is detected during the subsequent heating). Thus, to correctly perform the isothermal experiments, the selected T_c, must be higher than or equal to the $T_{c,min}$, i.e., $T_c \geq T_{c,min}$. 30 Here, we performed the isothermal experiments taking as a starting point $T_{c,min}$. Afterward, $T_c > T_{c,min}$ was employed, and up to 10 values of T_c per sample were used. The isothermal experiments consisted of erasing the thermal history, cooling from the melt (at 60 °C/min) to T_c, and holding the sample at T_c enough time to achieve a complete crystallization. Afterward, a heating scan at 20 °C/min was performed to record the melting behavior of the sample.

Simultaneous Wide-Angle and Small-Angle X-ray Scattering (WAXS/SAXS)

The samples (n_{CH2} = 6 to 12) were inserted in aluminum DSC pans and were examined under non-isothermal conditions by simultaneous WAXS/SAXS, using beamline BL11-NCD in the ALBA Synchrotron radiation facility (Barcelona, Spain). The DSC pans were placed inside a hot stage equipped with a liquid nitrogen cooling system (Linkam THMS600). For all the samples, the WAXS/SAXS patterns were collected during heating from 25 °C to T_mf ($T_{mf} = T_{mf} + 40°C$), employing a scanning rate of 20 °C/min. A 12.4 keV (λ=1.0 Å) X-ray source was employed. For WAXS measurements, a Rayonix LX255-HS detector was used, with an 85 x 255 mm^2 (pixel size 40x40 μm^2) active area and the sample-to-detector distance set to 196.14 mm with 30.33° tilt angle. The SAXS measurements were performed in a Pilatus 1M detector (from Dectris), with an active area of 168.7 x 179.4 mm^2 (pixel size 172x172 μm^2). The sample-to-detector distance was set to 6790 mm with a 0° tilt angle. Silver behenate (SAXS) and chromium (III) oxide (WAXS) were employed for calibration purposes.

The C16 sample was analyzed in the Shanghai Synchrotron Radiation Facility (SSRF), with the same procedure described above and a wavelength of 1.24 Å. A Pilatus 2M detector was used for SAXS, and a Pilatus 900 K detector was used for WAXS, respectively. Both with a pixel size of 172 x 172 μm^2. The sample-to-detector distance for WAXS was 173.24 mm and for SAXS 2191.1 mm. An exposure time of 5 seconds and a period of 6 seconds were used, allowing taking patterns every 2 °C.

X-ray Powder Diffraction (XRD)

XRD experiments were performed at RT. Two sets of samples were used: as synthesized (powder, directly from synthesis after purification by dissolution/precipitation and drying) and samples with a previous thermal history (inside DSC pans).

Samples without thermal history

The XRD experiments at RT were performed in a Rigaku XRD. The samples were scanned at a rate of 2 °/minute in the range of 5 to 60°. The samples, in powder (directly from synthesis), were placed into the cavity of a glass holder (i.e., until filled), which was carefully cleaned with alcohol. Then, the sample was gently pressed with a glass cover to obtain a flat surface.

Samples with previous thermal history

For these samples, the experiments were performed in an XRD P3 PAnalytical EMPYREAN equipment in its transmission mode, using the range of 5 to 60° and 200 seconds per step. The samples were previously prepared in DSC pans filled with approximately 20 to 30 mg of sample. In the DSC 8500 (see details in DSC section), the samples were heated until 150 °C for 3 minutes to erase their thermal history. Subsequently, the samples were cooled at different cooling rates: 1, 20, and 50 °C/min (high cooling rate) until – 60 °C. Finally, the samples were removed from the DSC at RT and tested in the XRD equipment.

Additionally, for C10 and C12 samples, an isothermal test was performed at high and low crystallization temperatures. For the C10 sample, the temperatures and times used were: 68 °C for 30 minutes and 73 °C for 90 minutes. For the C12 sample, we selected 73 °C for 30 minutes and 77 °C for 90 minutes.

3. Results and discussion

3.1.Non-isothermal DSC

Figure 1 shows the cooling (Figure 1a) and second heating (Figure 1b) DSC scans performed at 20 °C/min. All the samples show a single crystallization (T_c) and melting (T_m) peaks. Their values are listed in Table 2 and plotted as a function of the CH_2 number, n_{CH2}, in Figure 2.

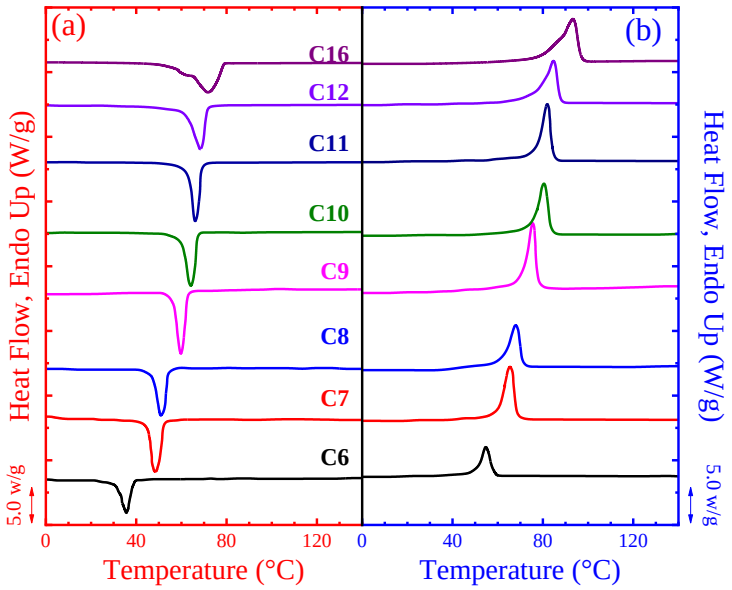

Figure 1. (a) cooling and (b) second heating DSC scans for all the samples (at a constant rate of 20 ºC/min).

Figure 1 shows that both T_c and T_m increase as n_{CH2} increases in two ways, depending on the n_{CH2} (see Figure 2), as we discuss below. Considering the crystallization and melting enthalpies (i.e., ΔH_c and ΔH_m), from Figure 1, we have calculated the percentage of crystallinity (X_c), using Eq. 1.

$$X_c = \frac{\Delta H_m}{\Delta H_m^0} \tag{1}$$

where ΔH_m is the enthalpy of fusion of the polyethers (see Table 2) (we also used the crystallization enthalpy (ΔH_c) for comparison purposes), and ΔH_m^0 is the equilibrium melting enthalpy of the polyethers (see Table 2). The ΔH_m^0 was calculated according to the group contribution semi-empirical theory established by Van Krevelen31 (see Section

S1). Table 2 shows the obtained X_c values (i.e., from both crystallization (X_{cc}) and melting (X_{cm}) enthalpies) and all the thermal properties determined from Figure 1.

Table 2. Calorimetric properties obtained for the samples shown in Figure 1 at 20 ºC/min scanning rates.

n_{CH2}	T_c (°C)	ΔH_c (J/g)	T_m (°C)	ΔH_m (J/g)	$\Delta H_{m(100\%)}$ (J/g)*	X_{cc} (%)	X_{cm} (%)
6	35	75	54.9	83	250	30	33
7	48	127	65.5	134	254	50	53
8	50.8	115	67.9	125	258	45	48
9	59.4	140	75.6	147	261	54	56
10	63.9	135	80.4	142	263	51	54
11	66.2	128	81.9	138	265	48	52
12	68.4	157	84.7	166	266	59	62
16	75.1	187	89.0	187	271	69	69

*Calculated following the Van Krevelen Group contribution method (see Section S1 in SI)

Figure 2 shows the T_c and T_m values, their enthalpies (ΔH), and the X_c values, determined from Figure 1 and reported in Table 2, as a function of n_{CH2}.

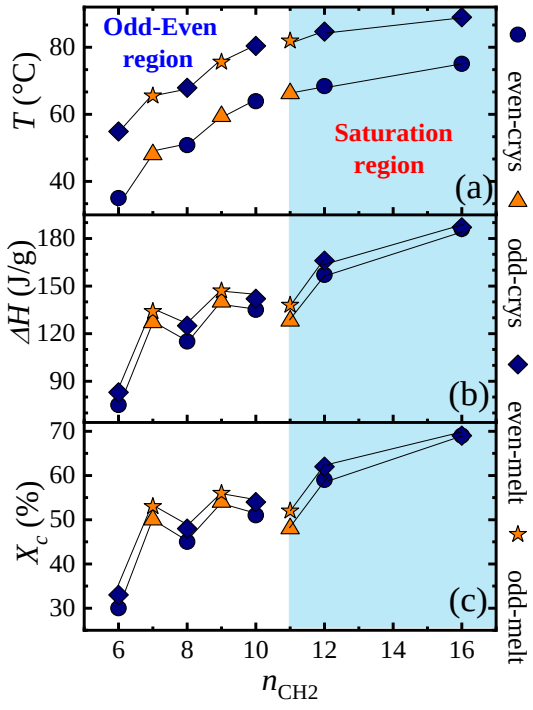

Figure 2. (a) Temperature (T, either T_m or T_c values) (b) Enthalpy (ΔH, either ΔH_m or ΔH_cvalues) and (c) Crystallinity (X_c, either X_{cc} or X_{cm} values) as a function of n_{CH2}. Samples were cooled from the melt at 20 ºC/min and then heated at the same scanning rate.

Figure 2 shows two different regions describing different trends. For n_{CH2} = 6 to 10, the T, ΔH, and X_c values increase as n_{CH2} increases, with the odd (n_{CH2} = 7 and 9) samples exhibiting higher values than the even ones, thus deviating from a linear increase. Here, we refer to this behavior (i.e., odd sample properties > even sample properties) as an alternation in properties that is typical of the odd-even region of calorimetric behavior. In contrast, for n_{CH2} > 10, such alternation disappears as calorimetric properties saturate, and a linear increase of T values as the n_{CH2} increases is observed. These two behaviors are indicated in Figure 2; the *odd-even* region (n_{CH2} = 6 to 10) and the *saturation* region (n_{CH2} = 11 to 12, and 16). Due to its crystalline structure, the C10 sample is considered within the odd-even region under this crystallization condition, i.e., non-isothermal crystallization at 20 ºC/min (see Section 3.3 for more details). Similar results were reported previously in linear aliphatic polycarbonates.22

Figure 2 shows that the alternation of T_c and T_m in the *odd-even* region is weak compared to other materials (e.g., polyamides, polyesters, and polycarbonates). This behavior corresponds to the influence of the oxygen groups, –O–, that establish weaker intermolecular interactions compared to other functional groups (i.e., carbonates, esters, and amides). Van Krevelen31 designed a molar contribution function to predict some of the properties of polymeric materials, e.g., melting temperature, based on the individual contribution of each chemical component in the monomeric unit. Considering these contributions, the –O– effect is lower (i.e., 0.3 K.kg/mol) than the –NH–CO–NH– groups (i.e., 2.5 K.kg/mol) effect that has the most substantial impact. From an experimental point of view, the weaker influence of the ether groups is reflected in the melt memory effect. Sangroniz et al.32 found that at n_{CH2} = 6, the melt memory effect (i.e., related to the width of *Domain IIa*) totally disappears for aliphatic polyethers but it is still is present for polyesters, polycarbonates, and polyamides.

For comparison purposes, we determine the theoretical equilibrium melting temperature (T_{mt}^0) of all the samples (i.e., by applying the molar contribution function, see Section S1 and Figure S1 on the SI), and plotted them as a function of n_{CH2}. The trend exhibited by T_{mt}^0 vs. n_{CH2} curve (Figure S1) is similar to the one shown in Figure 2a,

evidencing the weaker influence of the ether group. On the other hand, such weak interaction generates a strong alternation of the crystalline structure (see Section 3.3).

The *saturation* region (i.e., n_{CH2} = 11 to 12, and 16) (see Figure 2) is characterized by the absence of alternation in T_m between even and odd members. This saturation is caused by the increasing influence of the methylene groups, as the functional group (in this case, ether linkages) influence decreases (the proportion of ether linkages decreases as n_{CH2} increases). Thus, the material tends towards a polyethylene (PE)-like molecular conformation, intermolecular packing,33 and structure in the saturation region. Structurally, it is expected that the saturation of the odd-even effect leads to an orthorhombic unit cell (PE-like unit cell) independently of n_{CH2} (odd vs. even), as in other works reported in the literature.19, 20, 22 In these works, the saturation in the properties and the structural saturation occur at the same n_{CH2}. Here, under certain crystallization conditions, we found a saturation on the calorimetric properties (e.g., T_c and T_m) at n_{CH2} = 11 and a "total" saturation (including calorimetric and structural saturation) at n_{CH2} = 16 (see Section 3.3).

Figure 2 exhibits an interesting and uncommon feature since the odd members display higher calorimetric properties than the even ones (note that this trend is evident in Figure 2b and c). In most of the polymers with the even-odd effect, higher calorimetric properties are found for the even members of a given polymer family. Only in limited cases, such as N-acyl L-alanines, the opposite trend (i.e., odd-even effect) is reported: higher properties for the odd members.34, 35 Sivaramakrishna et al.35 claim that the terminal methyl groups of opposing layers in N-acyl L-alanines are more tightly packed in the odd samples than the even ones. They suggest that this type of tight packing might be related to the tilted acyl chain packing. Therefore, the van der Waals interactions between methyl groups of opposite layers are different for the even and odd-chain length series. Alamo et al.19 provide the big picture of the odd-even effect for polyethylene with acetal groups precisely spaced, including data of precision polyacetals.20, 21 These authors explained the odd-even effect (for n_{CH2} < 10) through a favorable interlocking of the acetals in the odd samples crystals.19, 20 Here, the ether linkage can produce a similar effect, generating an odd-even effect.

Figures 2b and 2c evaluate the evolution of ΔH and X_c as a function of n_{CH2}. Even though the analysis of ΔH escapes from the aim of this work, it illustrates the differences between the odd-even effect and the saturated regions. Here, an alternation in the odd-

even region is found (i.e., the odd samples have higher ΔH and X_c than the even ones). This alternation is inverted (i.e., ΔH and X_c values of even samples are higher than odd ones) in the saturation region. Such a difference remarks that these calorimetric properties behave differently in each region. Similar differences were found in the behavior of the ΔH values for polycarbonates. 22 Badea et al. found an alternation of the ΔH in the saturation region in alkanediols. 36 The differences found by these authors are related to the different crystal structures and molecular conformation (i.e., monoclinic (even) vs. orthorhombic (odd), and *trans* (even) vs. *gauche* (odd) conformation).

3.2.Isothermal Crystallization Kinetics evaluated by DSC

The isothermal crystallization determined by DSC allows studying the overall (nucleation + growth) crystallization kinetics. The inverse of the half crystallization time ($1/\tau_{50\%}$), i.e., an experimental value directly proportional to the overall crystallization rate, was determined from the DSC isothermal curves and plotted vs. T_c for each sample in Figure 3a. The isothermal curves were analyzed with the Avrami theory 37 (see Figure S2 on the SI), determining the Avrami index, n, and the isothermal crystallization rate constant value, $K^{1/n}$ (see Figure S3). As expected, the latter displayed the same trend as the $1/\tau_{50\%}$ vs. T_c curves (see Figure 3a). To consider the influence of the n_{CH2} value on the crystallization kinetics, the T_c values needed to reach a constant value of $1/\tau_{50\%}$= 0.5 min^{-1} were determined and plotted as a function of n_{CH2} in Figure 3b.

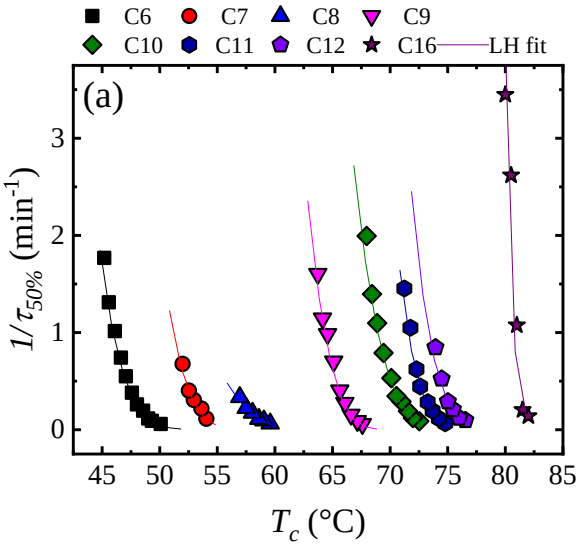

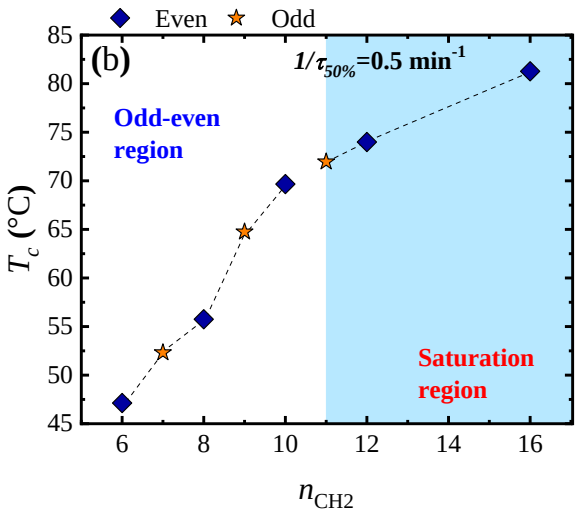

Figure 3. (a) $1/\tau_{50\%}$ vs. T_c, and (b) the T_c (at constant $1/\tau_{50\%}$ = 0.5 min^{-1}) vs. n_{CH2}. Note that the solid lines were obtained by applying the Lauritzen and Hoffman theory[38, 39] (see Section S2 on the SI).

Figure 3a shows that as n_{CH2} increases, the $1/\tau_{50\%}$ vs. T_c curves are shifted to higher T_c, in both, *odd-even* region (n_{CH2} = 6 to 10) and *saturation* (n_{CH2} = 11 to 16) region. For the *odd-even* region, the shift to higher T_c, instead of a strong alternation in the T_c values (e.g., higher T_c for the odd members), is attributed to the weak influence of the ether linkages. For "stronger" functional groups, a strong alternation of $1/\tau_{50\%}$ vs. T_c curves (e.g., even members at higher T_c than the odd members) is expected. This alternation in the crystallization kinetics has only been reported in a few works. [22, 40, 41]

Papageorgiou and Bikiaris[40] found that polypropylene succinate (PPS, n_{CH2} = 3, odd) has the slowest crystallization rate between polybutylene succinate (PBS, n_{CH2} = 4, even) and polyethylene succinate (PES, n_{CH2} = 2, even). They attributed this alternation (i.e., PPS < PES < PBS) to the even-odd effect in poly (alkylene succinate)s and the flexible butylene units in the chemical structure of the PBS. In aliphatic polycarbonates, we previously reported that the $1/\tau_{50\%}$ vs. T_c curves for n_{CH2} = 6 and 8 are shifted to higher T_c compared to n_{CH2} = 7 in the even-odd region (n_{CH2} = 6 to 9).[22] The different conformations and crystalline structures between even and odd samples explained this behavior. [22]

Figure 3b shows a detailed picture of the slight alternation of the T_c (at a constant $1/\tau_{50\%}$ = 0.5 min^{-1}) values as n_{CH2} increases for n_{CH2} = 6 to 10, as a result of the *odd-even effect*. Note that such alternation is not easy to detect in the $1/\tau_{50\%}$ vs. T_c curves. The behavior displayed by the T_c vs. n_{CH2} plot, in Figure 3b, is in line with the non-

isothermal experiments; hence the overall crystallization kinetics behavior of aliphatic polyethers can be divided into the *odd-even effect* (n_{CH2} = 6 to 10) region and a *saturation* region (n_{CH2} = 11, 12, and 16). In the *saturation* region, the crystallization kinetics resembles alkanes, since as n_{CH2} increases faster crystallization kinetics is obtained. Figure 3b shows that, in the saturation region, the T_c values increase linearly as n_{CH2} increases, evidencing the differences between the *odd-even* and the *saturation* region.

The Avrami theory was used to fit the isothermal data, employing the Crystallization_Fit Origin ® App.42 We have obtained n values around 3 (see Figure S3 in the SI), which indicates the formation of spherulitic morphology via instantaneous nucleation.

So far, we have divided the thermal behavior into two regions: the *odd-even* and the *saturation* regions. Despite the small changes in the *odd-even* region, we will show a remarkable alternation in the crystalline structure of even and odd samples in the next section. Here we will show how the alternation of the crystalline structures is extended to the *saturation* region.

3.3.Structural characterization with WAXS and SAXS

The WAXS and SAXS patterns were taken at room temperature after creating a standard thermal history by cooling the samples from the melt at 20 ºC/min, reproducing the crystallization conditions employed in the non-isothermal DSC experiments (Figures 1-2). Figure 4 shows the WAXS patterns for all the samples at 25 ºC, whereas Figure S5 shows the WAXS patterns taken *in-situ* during the heating of the samples.

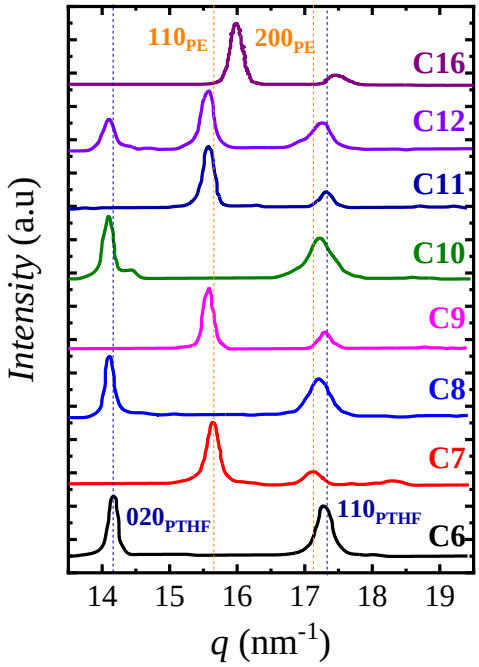

Figure 4. WAXS diffraction patterns of each polyether at 25 °C after creating a standard thermal history (cooling the samples from the melt at 20 ºC/min). The vertical dashed lines indicate the diffraction main planes of PE- and PTHF-like unit cells.

Figure 4 shows different WAXS patterns for the even and odd samples. In this work, the found diffraction peaks are correlated to the already reported structures of aliphatic polyethers with n_{CH2} = 6 to 10, and 12, by Kobayashi et al.29 The WAXS patterns of the even samples (n_{CH2} = 6, 8, and 10) displays two main peaks at q values of 14.2 and 17.3 nm^{-1} (2θ = 12.98 and 15.83°, respectively), which according to the literature, can be indexed to strong and very strong reflections of the *(020)* and *(110)* PTHF-type (monoclinic) planes, respectively.29 In contrast, for the odd samples (n_{CH2} = 7, 9, and 11) and the n_{CH2} = 16, the patterns displays two main peaks at q values of 15.6 and 17.1 nm^{-1} (2θ = 14.26 and 15.64°, respectively), which can be indexed to the very strong and strong reflections of the *(110)* and *(200)* PE-type (orthorhombic) planes, respectively.29 For n_{CH2} = 7, a less intense peak is observed at q ~ 18.3 nm^{-1} (2θ=16.75°). Despite this peak, which was also reported by Kobayashi et al.,29 the unit cell for the C7 sample can be also considered orthorhombic. In the case of n_{CH2} = 12, there are three prominent peaks, in which two of them, q = 15.6 and 17.1 nm^{-1}, can be indexed to an orthorhombic unit cell, and the remaining one, q = 14.2 nm^{-1}, to a

monoclinic unit cell. This is an interesting feature since the C12 belongs to the saturation region, and hence, a PE-like orthorhombic unit cell is expected[22].

The unit cell of the even samples (n_{CH2} = 6, 8, and 10) resembles the unit cell of the polytetrahydrofuran (PTHF) that is monoclinic, with crystal sizes of a = 0.559 nm, b = 0.890 nm, c (fiber axis) = 1.207 nm, and β = 134.2° with space group *C2/c-*C^6_{2h}. [29] The unit cell of the odd samples (n_{CH2} = 7, 9 and 11) and the C16 sample resemble the unit cell of the PE that is orthorhombic, with crystal sizes of a = 0.740 nm, b = 0.493 nm, and c (fiber axis) = 0.2534 nm, with space group *Pnam-*D^{16}_{2h}.[29]

The WAXS pattern of the C12 sample corresponds to a mixture of the PTHF-like (see that the *(020)* plane of the PTHF unit cell is present in Figure 4) and PE-like unit cell, in which the dominant crystalline structure (judging by the peaks intensity) is the PE one. A mixture of PE and PTHF-like unit cells was also found in linear aliphatic polyethers by Kobayashi et al.[29] for n_{CH2} = 10 and 12.

The conformational characterization of aliphatic polyethers family is reported in the literature.[29, 43] It has been found that the first four members (i.e., n_{CH2} = 1 to 4) exhibited helical structures for n_{CH2} = 1 and 2,[44] and *zigzag* conformation for n_{CH2} = 3, and 4.[45] The n_{CH2} = 5, have not been studied because of the difficulties for its synthesis.[6, 44] The molecular conformation for n_{CH2} > 5 is also *zigzag*, complicating a conformational analysis of the odd-even effect compared to samples that show more significant differences, e.g., *gauche* vs. *trans* conformations of the methylene groups. However, it is reported that aliphatic polyethers can adopt a PTHF or a PE-like conformation, depending on the n_{CH2} value (even (PTHF) vs. odd (PE)). The only difference between these conformations is the angle, ϕ, between the chains and the bc plane.

In both PTHF-like (i.e., even samples) and PE-like conformations, planar *zigzag* chains pass through the center and the corner of the unit cell. For the PTHF-like conformation, the *zigzag* planes of the molecular chains are parallel to bc. Therefore, the molecular packing for the PTHF makes an angle $\phi = 90^\circ$ with the bc plane, resulting in a PTHF-like unit cell. In contrast, for the PE-like conformation (i.e., odd samples), the *zigzag* chains make an angle of $\phi = 41^\circ$ with the bc plane, resulting in a PE-like unit cell. In the *odd-even* region, i.e., low n_{CH2} values the PTHF-like packing is more stable, and in the *saturation* region, i.e., high n_{CH2} values, in which the influence of the oxygen group is weakened, the most stable is the PE-like packing.[29] The odd samples display a PE-like

packing independently of the n_{CH2} value, whereas the even samples can adopt either a PTHF or a PE-like packing, depending on the n_{CH2} value.29

When the samples are crystallized from the melt, only the even samples, n_{CH2} = 6, 8, and 10, have a PTHF-like packing. As the n_{CH2} increases, the packing on the even samples changes to a mixture of a PE-like and PTHF-like packing, for n_{CH2} = 12, and a PE-like packing (i.e., due to structural saturation) for n_{CH2} = 16. In contrast, the odd samples, n_{CH2} = 7, 9, and 11, maintain a PE-like packing independent of the n_{CH2}, as aliphatic polycarbonates.22 The explanation of the mixed structure for n_{CH2} = 12 needs further investigation. However, we can speculate that it is related to the ϕ angle with the bc plane in between 90 (PTHF-like) and 41˚ (PE-like), constituting a boundary condition between the structural *odd-even* and *saturation* region.

We have calculated the d-spacing, by using the q values in Figure 4, according to Bragg's law. Figure 5 shows the d-spacing as a function of the n_{CH2}. Table S2 listed the q values and the calculated d-spacings.

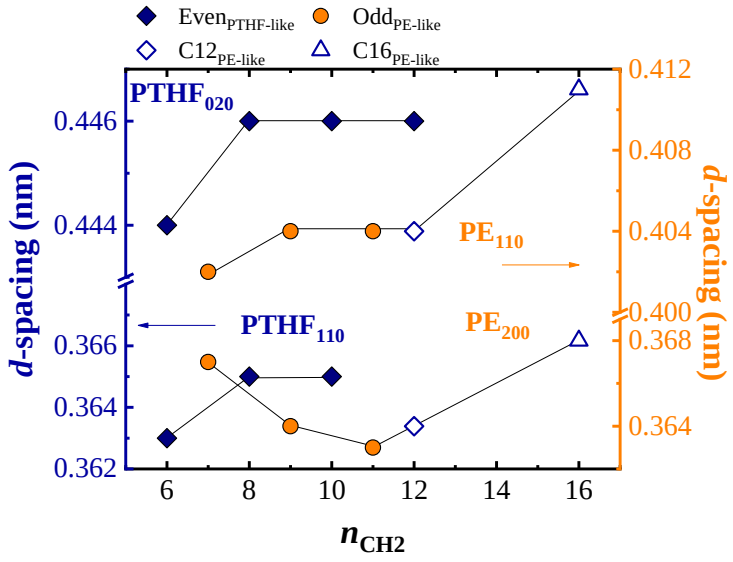

Figure 5. Interplanar distance (*d-spacing*) vs. n_{CH2} for all reflections at 25 ˚C for each polyether.

Figure 5 shows that the d-spacing changes as n_{CH2} increases. In the *odd-even* region, the d-spacing (d_{110} and d_{020}) of even samples (i.e., PTHF-like) significantly increase at low n_{CH2} = 6 to 8, and only slightly increases (i.e., d_{110}) at high n_{CH2} = 8 to 10. The odd samples (see n_{CH2} = 7 to 9) display similar behavior, but with smaller changes than the even ones, related to their more efficiently packed structure.

In the *saturation* region, n_{CH2} = 11 to 16, the methylene units have more weight than the ethers groups, adopting a PE-like packing and structure. Thus, the d-spacing changes are lower compared to the *odd-even* region. The C12 sample displays d-spacings corresponding to PTHF-like and PE-like unit cells but similar to the C11 and C10 samples. The C16 exhibits higher d-spacings due to the increases in n_{CH2}.

To further understand the structural behavior, we performed the XRD test, with varied thermal histories, to understand the structural alternation (see Section 3.4)

SAXS Analysis

In-situ SAXS patterns were taken at the synchrotron source. A single main peak characterizes all the SAXS patterns due to the scattering caused by the periodic lamellar structure (i.e., long period). In Figure 6, we take, as an example, the Lorentz-corrected SAXS intensity profiles as a function of the scattering vector q during the heating of the C6 sample.

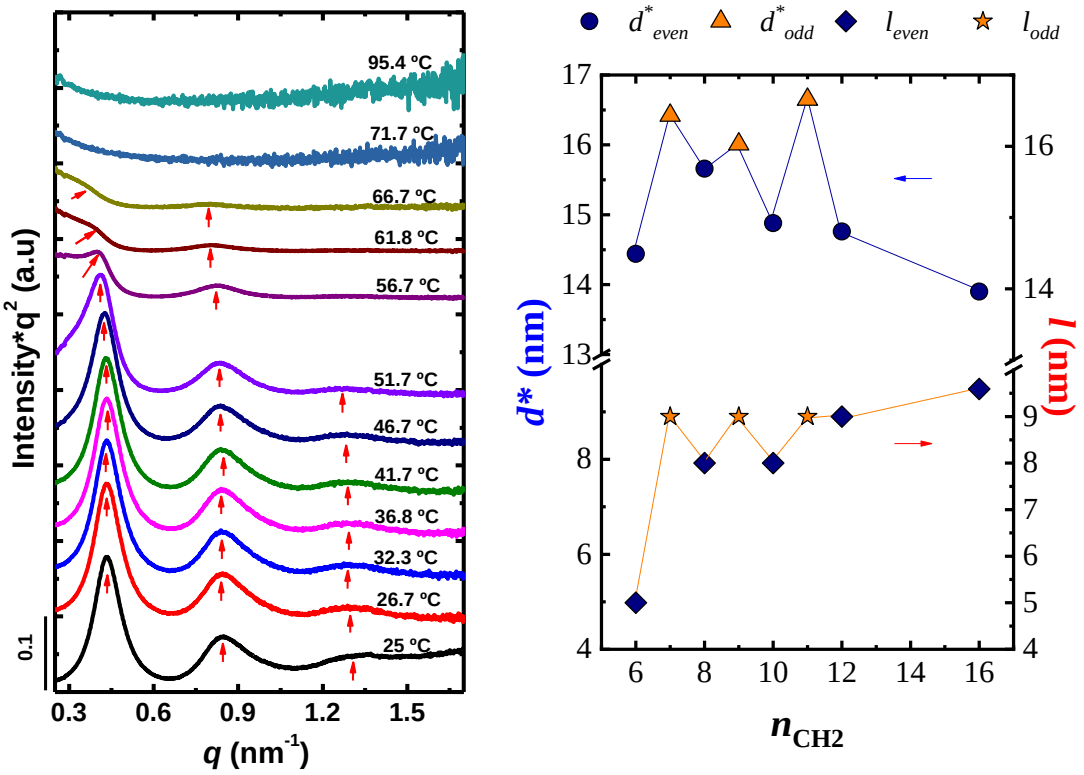

Figure 6. Lorentz-corrected SAXS profiles for C6, with intensity as a function of scattering vector (left). Data taken of samples cooled from 25 °C to 95 °C at 20 °C/min. Long period (d^*) and lamellar thickness (l) as a function of n_{CH2} (right).

Figure 6 shows three peaks for low temperatures. The main signal is at q = 0.43 nm^{-1}, and two weaker signals are at q = 0.83 nm^{-1} and q =1.29 nm^{-1}, respectively. These peaks exhibit a 1:2:3 relationship in q, corresponding to a lamellar structure, as expected. The long period (d^*) at different temperatures was estimated by Equation 2. The q_{max} (i.e., q value of the main signal) values were taken from the Lorentz corrected plots (*Intensity*.q^2 versus q).

$$d^* = \frac{2\pi}{q_{max}} \quad (2)$$

The d^* values at different temperatures were calculated for each of the polyethers (Figure S6 displayed their SAXS during heating) and are represented in Figure S7. Figure 6 (right) shows the $d^*$and lamellar thickness (l) values as a function of n_{CH2}. The lamellar thickness (l) was estimated using the following approximation (Equation 3).

$$l = d^* . X_c \quad (3)$$

where X_c is the crystalline mass fraction (see Figure S8), listed in Table 1. Table S3 lists the calculated d^* and l values. Figure 6 (right) shows higher d^* values (left *y*-axis) for the odd samples (16.0 – 16.7 nm) than the even ones (13.9 – 15.7 nm). We observe the same trend during heating (see Figure S7), and it is in line with the *odd-even* alternation (i.e., higher values for the odd members) observed in other properties. The l values (right *y*-axis) are higher for the odd samples than the even ones in the *odd-even* region. For the saturation region, the l values only slightly change or remain unchanged as n_{CH2} increases. The behavior of l vs. n_{CH2} is in line with the findings on the crystallization behavior.

3.4.Influence of the thermal history: XRD experiments

Chain packing in the odd samples is stable, resembling PE-like packing, independently of n_{CH2} value. The even samples display a chain length-dependent behavior, since their packing shifts from a PTHF-like packing, at low n_{CH2} (i.e., n_{CH2} = 6, 8, and 10), to a PTHF-like + PE-like packing at n_{CH2} = 12 and a PE-like packing at high n_{CH2} (i.e., n_{CH2} = 16). When different crystallization conditions are employed, the

chain packing of the odd samples remains unchanged, whereas alterations have been reported (and studied) in the even samples.

Yoshida et al.[46] found that a C8 polyether sample forms a mixture of PE and PTHF-like unit cells when it is crystallized from solution and forms PTHF-like crystals when it is crystallized from the melt. Similarly, Fernandez-Bermudez and Balta-Calleja[47] found both types of crystals (i.e., PE and PTHF-like crystals) in a C10 polyether sample crystallized from solution, whereas from the melt, the C10 forms PE-like crystals.[29] The reported results[46, 47] for the C8 and C10 samples, crystallized from the melt, are in line with our results (see Figure 4). In contrast, Kobayashi et al.[29] found both types of crystals in the C8, C10, and C12 samples, crystallized from the melt.

In our previous work,[6] WAXS measurements were performed in the samples as synthesized (i.e., crystallized during precipitation from solution and dried). In the *odd-even* region, an alternation between PTHF-like (n_{CH2} = 6 and 8) and PE-like (n_{CH2} = 7) crystals was recorded, whereas in the *saturation* region, all the samples (n_{CH2} = 9 to 12) formed PE-like crystals. In the present work, we found that when a standard thermal history is created (by cooling from the melt at 20 ºC/min), the odd samples (n_{CH2} = 7, 9, 11) show PE-like crystals, whereas the even samples show a different type of crystals. For n_{CH2} = 6, 8, and 10, PTHF-like crystals were found. The C12 crystallized with a mixture of PTHF- and PE-like crystals, and the C16 with PE-like crystals. Such behavior seems to indicate a thermal history influence, which we decided to investigate with XRD experiments.

Measurements at different cooling rates

Different cooling rates, 1, 20, and 50 °C/min, were used to crystallize the samples from the melt, creating different thermal histories. Afterwards, XRD measurements were taken at RT (see Figure 7). The as synthesized samples, i.e., precipitated from solution and dried, were also studied. After measuring all the samples at RT, subsequent heating scans were performed in the DSC (see Figure S9 in the SI).

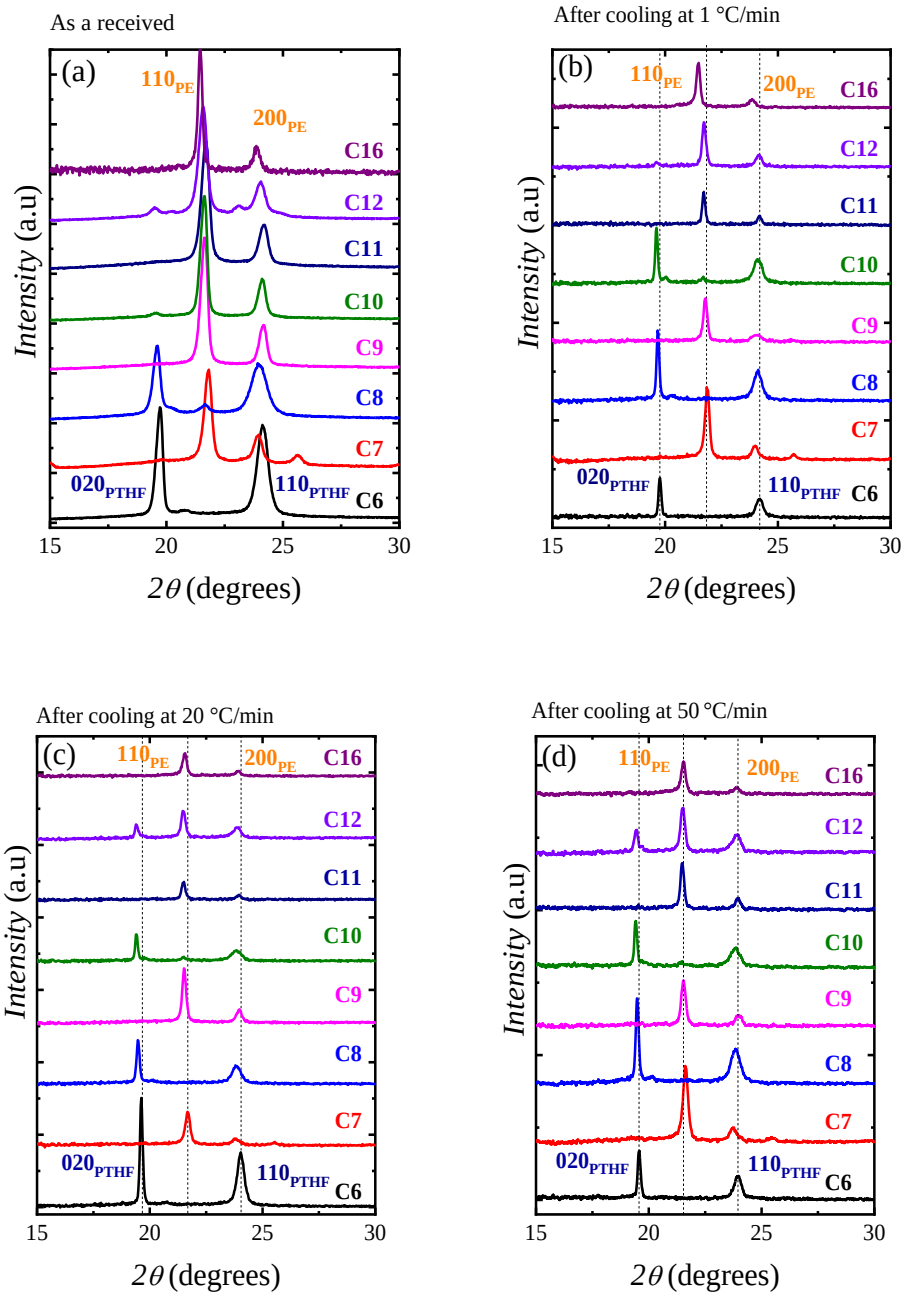

Figure 7. XRD taken at RT in samples previously prepared at different cooling rates. (a) As a received sample in powder. Samples crystallized from the melt at (b) 1, (c) 20, and (d) 50 °C/min.

Figure 7a shows that the as synthesized sample forms PTHF-like crystals for n_{CH2} = 6 and 8, and PE-like crystals for n_{CH2} = 7, and 9 to 16. The XRD patterns are in line with the WAXS ones, taken at the same crystallization conditions. Differences in the XRD patterns beyond the corresponding to the PE-like and PTHF-like unit cell were not found at $2\theta > 30°$, in neither of the crystallization conditions shown in Figure 7; however, a deeper study, such as the one performed by Tasaki et al.[23, 24] might provide further

information. However, such a detailed crystallographic study is beyond the scope of the present contribution..

The XRD for as synthesized samples reveals that the limits of the *odd-even* and *saturation* region changed. The n_{CH2} = 8 to 9 are in the *odd-even* region, and the n_{CH2} = 10 to 16 in the *saturation* region. When the samples are crystallized from the melt (see Figures 7b, c, and d), the PE-like crystals are limited to the odd samples (i.e., n_{CH2} = 7, 9, and 11), and the even sample with n_{CH2} = 16. In contrast, PTHF-like crystals are observed in the even samples (i.e., n_{CH2} = 6, 8, and 10). In the case of the C12 sample, a mixture of crystal structures is observed in which the dominant reflections correspond to the PE-like crystals, whereas the PTHF-like crystals peaks increase as the cooling rate increases. Similar results were found in the XRD measurements in the C10 and C12 samples after isothermal crystallization at different T_c (see Figure S10 in Section S4). Higher T_c favored PE-like crystals in the C12 sample, whereas the PTHF-like crystals are formed independently of the T_c for the C10 sample.

The rate-dependent behavior of the even samples with n_{CH2} = 10 and 12 indicates that the oxygen group still influences the chain packing, limiting the total structural saturation of the odd-even effect. It might be speculated that the ϕ angle with the bc plane (i.e., 90º for even samples and 41º for odd ones) varies suddenly, in the odd-even region, between 90º (even) and 41º (odd). Afterward, at n_{CH2} values closer to the saturation region, ϕ might varied progressively in the even samples (note that odd samples maintain a ϕ = 41º independently of the n_{CH2} value), taking values in between 90º and 41º, affecting the crystalline structure. Finally, in the saturation region, the *trans* chains take a ϕ = 41º resembling a PE-like packing. From a structural point of view, the saturation of the odd-even effect occurs at n_{CH2} > 12, since the C16 (n_{CH2} = 16) sample maintains its PE-like structure, independently of the thermal history. The results suggest that the C10 and C12 can be in the *odd-even* region or the *saturation* region, depending on the adopted conformation at a specific crystallization condition, constituting a boundary between the regions. We found that the *odd-even* and *saturation* region limits are well established in the thermal and crystallization properties. Interestingly, from a structural point of view, the even samples can adopt either PTHF- or PE-like packing, altering the limits of the saturation region.

4. Conclusions

A series of aliphatic polyethers, in a wide range of chain length (n_{CH2} = 6 to 12, and 16), were studied by differential scanning calorimetry (DSC), wide-and small-angle X-ray scattering (WAXS and SAXS) and X-ray diffraction (XRD) experiment. Non-isothermal DSC experiments reveal a weak *odd-even effect* for n_{CH2} = 6 to 10, in which the odd (n_{CH2} = 7 and 9) samples show higher crystallization and melting temperatures than the even (n_{CH2} = 6, 8, and 10) ones. This effect is saturated for n_{CH2} = 11 to 12, and 16, in which a linear increase of the calorimetric properties as n_{CH2} increases was found. An *odd-even* region and a *saturation* region were also found under isothermal conditions. The *odd-even* region is explained by the weak dipole interactions imposed by the oxygen group and the *saturation* region, by the increasing influence of the methylene groups (hence the dilution of the oxygen group influence) as n_{CH2} increases.

The structure of all the samples was investigated with X-ray experiments. Interestingly, despite the weak interactions, the s*tructural alternation* in the *odd-even* region is strong. The even samples (n_{CH2} = 6, 8, and 10) exhibit monoclinic unit cells, and the odd ones (n_{CH2} = 7 and 9) orthorhombic unit cells. The *saturation* region displays particular features since it depends on the thermal history. The odd C11 sample maintains an orthorhombic unit cell independently on the crystallization conditions. In contrast, the even C10 and C12 can adopt monoclinic, orthorhombic, or mixed structures (i.e., C12 sample) depending on the thermal history, affecting the limits of the *saturation* region. Hence, *structural saturation* is reached only for the C16 sample, which adopts the expected orthorhombic structure independently of the thermal history.

ACKNOWLEDGMENTS

We would like to thank the financial support provided by the BIODEST project; this project has received funding from the European Union's Horizon 2020 research and innovation programme under the Marie Sklodowska-Curie grant agreement no. 778092. This work was also supported by Grant PID2020-113045GB-C21 funded by MCIN/AEI/10.13039/501100011033. This work has also received funding from the Basque Government through grant IT1309-19. R.A.P.-C is supported by the China Postdoctoral Science Foundation (2020M670462), and National Natural Science Foundation of China (NSFC) (52050410327). The support of the ALBA (2020024169) and SSRF synchrotron facility is gratefully acknowledged.

5. References

1. Klein, R.; Wurm, F. R. Aliphatic Polyethers: Classical Polymers for the 21st Century. *Macromolecular Rapid Communications* **2015,** 36 (12), 1147-1165 DOI: 10.1002/marc.201500013.
2. Saunders, K. J., Aliphatic Polyethers. In *Organic Polymer Chemistry: An Introduction to the Organic Chemistry of Adhesives, Fibres, Paints, Plastics and Rubbers*, Springer Netherlands: Dordrecht, 1988; pp 171-190.
3. Perry, S.; Hibbert, H. Studies on Reactions Relating to Carbohydrates and Polysaccharides. LXI. The Mechanism of Polymerization of Ethylene Oxide1. *Journal of the American Chemical Society* **1940,** 62 (10), 2599-2604 DOI: 10.1021/ja01867a005.
4. Vandenberg, E. J. Organometallic catalysts for polymerizing monosubstituted epoxides. *Journal of Polymer Science* **1960,** 47 (149), 486-489 DOI: 10.1002/pol.1960.1204714947.
5. Dreyfuss, M. P.; Dreyfuss, P. A 'living' polymer after cationic initiation. *Polymer* **1965,** 6 (2), 93-95 DOI: https://doi.org/10.1016/0032-3861(65)90018-2.
6. Basterretxea, A.; Gabirondo, E.; Jehanno, C.; Zhu, H.; Flores, I.; Müller, A. J.; Etxeberria, A.; Mecerreyes, D.; Coulembier, O.; Sardon, H. Polyether Synthesis by Bulk Self-Condensation of Diols Catalyzed by Non-Eutectic Acid–Base Organocatalysts. *ACS Sustainable Chemistry & Engineering* **2019,** 7 (4), 4103-4111 DOI: 10.1021/acssuschemeng.8b05609.
7. Basterretxea, A.; Gabirondo, E.; Flores, I.; Etxeberria, A.; Gonzalez, A.; Müller, A. J.; Mecerreyes, D.; Coulembier, O.; Sardon, H. Isomorphic Polyoxyalkylene Copolyethers Obtained by Copolymerization of Aliphatic Diols. *Macromolecules* **2019,** 52 (9), 3506-3515 DOI: 10.1021/acs.macromol.9b00469.
8. Knop K, H. R., Fischer D, Schubert US. . Poly(ethylene glycol) in drug delivery: pros and cons as well as potential alternatives. *Angew Chem Int Ed Engl.* **2010,** 49 (36), 20 DOI: 10.1002/anie.200902672
9. Olmedo-Martínez, J. L.; Meabe, L.; Basterretxea, A.; Mecerreyes, D.; Müller, A. J. Effect of Chemical Structure and Salt Concentration on the Crystallization and Ionic Conductivity of Aliphatic Polyethers. *Polymers* **2019,** 11 (3), 452.
10. Engels, H.-W.; Pirkl, H.-G.; Albers, R.; Albach, R. W.; Krause, J.; Hoffmann, A.; Casselmann, H.; Dormish, J. Polyurethanes: Versatile Materials and Sustainable Problem Solvers for Today's Challenges. *Angewandte Chemie International Edition* **2013,** 52 (36), 9422-9441 DOI: 10.1002/anie.201302766.
11. Basterretxea, A.; Lopez de Pariza, X.; Gabirondo, E.; Marina, S.; Martin, J.; Etxeberria, A.; Mecerreyes, D.; Sardon, H. Synthesis and Characterization of Fully Biobased Copolyether Polyols. *Industrial & Engineering Chemistry Research* **2020,** 59 (23), 10746-10753 DOI: 10.1021/acs.iecr.0c00723.
12. Uhrich, K. E.; Hawker, C. J.; Frechet, J. M. J.; Turner, S. R. One-pot synthesis of hyperbranched polyethers. *Macromolecules* **1992,** 25 (18), 4583-4587 DOI: 10.1021/ma00044a019.
13. Dannecker, P.-K.; Biermann, U.; von Czapiewski, M.; Metzger, J. O.; Meier, M. A. R. Renewable Polyethers via GaBr3-Catalyzed Reduction of Polyesters. *Angewandte Chemie International Edition* **2018,** 57 (28), 8775-8779 DOI: 10.1002/anie.201804368.
14. Monnier, X.; Marina, S.; Lopez de Pariza, X.; Sardón, H.; Martin, J.; Cangialosi, D. Physical Aging Behavior of a Glassy Polyether. **2021,** 13 (6), 954.
15. Pérez-Camargo, R. A.; Arandia, I.; Safari, M.; Cavallo, D.; Lotti, N.; Soccio, M.; Müller, A. J. Crystallization of isodimorphic aliphatic random copolyesters: Pseudo-eutectic behavior and double-crystalline materials. *European Polymer Journal* **2018,** 101, 233-247 DOI: https://doi.org/10.1016/j.eurpolymj.2018.02.037.

16. Yang, K.; Cai, Z.; Jaiswal, A.; Tyagi, M.; Moore, J. S.; Zhang, Y. Dynamic Odd–Even Effect in Liquid n-Alkanes near Their Melting Points. *Angewandte Chemie International Edition* **2016,** 55 (45), 14090-14095 DOI: 10.1002/anie.201607316.
17. Costa, J. C. S.; Santos, L. M. N. B. F. Chain-Length Dependence of the Thermodynamic Behavior of Homologous α,ω-Disubstituted Alkanes. *Journal of Chemical & Engineering Data* **2019,** 64 (6), 2229-2246 DOI: 10.1021/acs.jced.9b00125.
18. Duer, M. J.; Roper, C. A solid-state NMR investigation of the odd–even effect in a series of liquid-crystal dimers. *Physical Chemistry Chemical Physics* **2003,** 5 (14), 3034-3041 DOI: 10.1039/b303475p.
19. Zhang, X.; Zuo, X.; Ortmann, P.; Mecking, S.; Alamo, R. G. Crystallization of Long-Spaced Precision Polyacetals I: Melting and Recrystallization of Rapidly Formed Crystallites. *Macromolecules* **2019,** 52 (13), 4934-4948 DOI: 10.1021/acs.macromol.9b00922.
20. Stempfle, F.; Ortmann, P.; Mecking, S. Long-Chain Aliphatic Polymers To Bridge the Gap between Semicrystalline Polyolefins and Traditional Polycondensates. *Chemical Reviews* **2016,** 116 (7), 4597-4641 DOI: 10.1021/acs.chemrev.5b00705.
21. Pemba, A. G.; Flores, J. A.; Miller, S. A. Acetal metathesis polymerization (AMP): A method for synthesizing biorenewable polyacetals. *Green Chemistry* **2013,** 15 (2), 325-329 DOI: 10.1039/C2GC36588J.
22. Pérez-Camargo, R. A.; Meabe, L.; Liu, G.; Sardon, H.; Zhao, Y.; Wang, D.; Müller, A. J. Even–Odd Effect in Aliphatic Polycarbonates with Different Chain Lengths: from Poly (Hexamethylene Carbonate) to Poly (Dodecamethylene Carbonate). *Macromolecules* **2020,** 54 (1), 259-271 DOI: 10.1021/acs.macromol.0c02374.
23. Tasaki, M.; Yamamoto, H.; Yoshioka, T.; Hanesaka, M.; Ninh, T. H.; Tashiro, K.; Jeon, H. J.; Choi, K. B.; Jeong, H. S.; Song, H. H.; Ree, M. H. Crystal structure analyses of arylate polyesters with long methylene segments and their model compounds on the basis of 2-D X-ray diffractions and infrared progression bands. *Polymer* **2014,** 55 (5), 1228-1248 DOI: https://doi.org/10.1016/j.polymer.2014.01.024.
24. Tasaki, M.; Yamamoto, H.; Yoshioka, T.; Hanesaka, M.; Ninh, T. H.; Tashiro, K.; Jeon, H. J.; Choi, K. B.; Jeong, H. S.; Song, H. H.; Ree, M. H. Microscopically-viewed relationship between the chain conformation and ultimate Young's modulus of a series of arylate polyesters with long methylene segments. *Polymer* **2014,** 55 (7), 1799-1808 DOI: https://doi.org/10.1016/j.polymer.2014.01.058.
25. Rulkens, R.; Koning, C., 5.18 - Chemistry and Technology of Polyamides. In *Polymer Science: A Comprehensive Reference*, Matyjaszewski, K., Möller, M., Eds. Elsevier: Amsterdam, 2012; pp 431-467.
26. Fernández, C. E.; Bermudez, M.; Versteegen, R. M.; Meijer, E. W.; Muller, A. J.; Muñoz-Guerra, S. Crystallization studies on linear aliphatic n-polyurethanes. *Journal of Polymer Science Part B: Polymer Physics* **2009,** 47 (14), 1368-1380 DOI: 10.1002/polb.21736.
27. Badea, E.; Gatta, G. D.; D'Angelo, D.; Brunetti, B.; Rečková, Z. Odd–even effect in melting properties of 12 alkane-α,ω-diamides. *The Journal of Chemical Thermodynamics* **2006,** 38 (12), 1546-1552 DOI: https://doi.org/10.1016/j.jct.2006.04.004.
28. Thalladi, V. R.; Nüsse, M.; Boese, R. The Melting Point Alternation in α,ω-Alkanedicarboxylic Acids. *Journal of the American Chemical Society* **2000,** 122 (38), 9227-9236 DOI: 10.1021/ja0011459.
29. Kobayashi, S.; Tadokoro, H.; Chatani, Y. Structural studies on polyethers, [□(CH2)m□O□]n. VI. The higher members with m = 6–10, 12. *Die Makromolekulare Chemie* **1968,** 112 (1), 225-241 DOI: 10.1002/macp.1968.021120120.

30. Lorenzo, A. T.; Arnal, M. L.; Albuerne, J.; Müller, A. J. DSC isothermal polymer crystallization kinetics measurements and the use of the Avrami equation to fit the data: Guidelines to avoid common problems. *Polymer Testing* **2007,** 26 (2), 222-231 DOI: https://doi.org/10.1016/j.polymertesting.2006.10.005.
31. Van Krevelen, D. W., CHAPTER 5 - CALORIMETRIC PROPERTIES. In *Properties of Polymers (Third Edition)*, Van Krevelen, D. W., Ed. Elsevier: Amsterdam, 1997; pp 109-127.
32. Sangroniz, L.; Sangroniz, A.; Meabe, L.; Basterretxea, A.; Sardon, H.; Cavallo, D.; Müller, A. J. Chemical Structure Drives Memory Effects in the Crystallization of Homopolymers. *Macromolecules* **2020,** 53 (12), 4874-4881 DOI: 10.1021/acs.macromol.0c00751.
33. Zhou, C.; Wei, Z.; Yu, Y.; Shao, S.; Leng, X.; Wang, Y.; Li, Y. Biobased long-chain aliphatic polyesters of 1,12-dodecanedioic acid with a variety of diols: Odd-even effect and mechanical properties. *Materials Today Communications* **2019,** 19, 450-458 DOI: https://doi.org/10.1016/j.mtcomm.2019.05.005.
34. Sivaramakrishna, D.; Swamy, M. J. Self-Assembly, Supramolecular Organization, and Phase Behavior of l-Alanine Alkyl Esters (n = 9–18) and Characterization of Equimolar l-Alanine Lauryl Ester/Lauryl Sulfate Catanionic Complex. *Langmuir* **2015,** 31 (35), 9546-9556 DOI: 10.1021/acs.langmuir.5b02475.
35. Sivaramakrishna, D.; Thirupathi Reddy, S.; Nagaraju, T.; Swamy, M. J. Self-assembly, supramolecular organization, and phase transitions of a homologous series of N-acyl-l-alanines (n=8–20). *Colloids and Surfaces A: Physicochemical and Engineering Aspects* **2015,** 471, 108-116 DOI: https://doi.org/10.1016/j.colsurfa.2015.02.025.
36. Badea, E.; Nowicka, B.; Della Gatta, G. Thermodynamics of fusion and sublimation for a homologous series of eleven alkane-α,ω-diols HO-(CH2)n-OH: Structure-related odd–even effect. *The Journal of Chemical Thermodynamics* **2014,** 68, 90-97 DOI: https://doi.org/10.1016/j.jct.2013.08.019.
37. Avrami, M. Granulation, Phase Change, and Microstructure Kinetics of Phase Change. III. *The Journal of Chemical Physics* **1941,** 9 (2), 177-184 DOI: 10.1063/1.1750872.
38. Lauritzen, J. I.; Hoffman, J. D. Theory of Formation of Polymer Crystals with Folded Chains in Dilute Solution. *J. Res. Natl. Bur. Stand., Sect. A* **1960,** 64A (1), 73-102 DOI: http://dx.doi.org/10.6028/jres.064A.007.
39. Hoffman, J. D.; Lauritzen, J. I. Crystallization of Bulk Polymers With Chain Folding: Theory of Growth of Lamellar Spherulites *J. Res. Natl. Bur. Stand., Sect. A* **1961,** 65A (4), 297-336 DOI: http://dx.doi.org/10.6028/jres.065A.035.
40. Papageorgiou, G. Z.; Bikiaris, D. N. Crystallization and melting behavior of three biodegradable poly(alkylene succinates). A comparative study. *Polymer* **2005,** 46 (26), 12081-12092 DOI: https://doi.org/10.1016/j.polymer.2005.10.073.
41. Soccio, M.; Lotti, N.; Finelli, L.; Gazzano, M.; Munari, A. Aliphatic poly(propylene dicarboxylate)s: Effect of chain length on thermal properties and crystallization kinetics. *Polymer* **2007,** 48 (11), 3125-3136 DOI: https://doi.org/10.1016/j.polymer.2007.04.007.
42. OriginLab Crystallization Fit. https://www.originlab.com/fileExchange/details.aspx?fid=597 (March 09, 2021),
43. Makino, D.; Kobayashi, M.; Tadokoro, H. Structural studies of polyethers [· (CH2)m · O ·]n · XI. Skeletal vibrations of planar zigzag polyethers. *Spectrochimica Acta Part A: Molecular Spectroscopy* **1975,** 31 (9), 1481-1495 DOI: https://doi.org/10.1016/0584-8539(75)80205-4.

44. Tadokoro, H. Structure and properties of crystalline polymers. *Polymer* **1984,** 25 (2), 147-164 DOI: https://doi.org/10.1016/0032-3861(84)90321-5.
45. Bunn, C. W.; Holmes, D. R. Chain configurations in crystals of simple linear polymers. *Discussions of the Faraday Society* **1958,** 25 (0), 95-103 DOI: 10.1039/DF9582500095.
46. Yoshida, S.; Suga, H.; Seki, S. Thermodynamic Studies of Solid Polyethers. IV. Poly(octamethylene oxide), –[–(CH2)8O–]–n. *Polymer Journal* **1973,** 5 (1), 33-40 DOI: 10.1295/polymj.5.33.
47. Fernández Bermúdez, S.; Baltá Calleja, F. J. Poly(decamethylene oxide) single crystals from dilute solution. *Colloid and Polymer Science* **1975,** 253 (1), 1-3 DOI: 10.1007/bf01419250.